

## STUDY OF RIBBON SEPARATION OF A FLARE ASSOCIATED WITH A QUIESCENT FILAMENT ERUPTION

HAIMIN WANG,<sup>1,2,3</sup> JIONG QIU,<sup>3</sup> JU JING,<sup>2,3</sup> AND HONGQI ZHANG<sup>1</sup>

Received 2003 February 14; accepted 2003 April 19

### ABSTRACT

In this paper, we present a detailed study of a two-ribbon flare in the plage region observed by Kanzelhoehe Solar Observatory (KSO), which is one of the stations in our global  $H\alpha$  network. We select this event due to its very clear filament eruption, two-ribbon separation, and association with a fast coronal mass ejection (CME). We study the separation between the two ribbons seen in  $H\alpha$  as a function of time and find that the separation motion consisted of a fast stage of rapid motion at a speed of about  $15 \text{ km s}^{-1}$  in the first 20 minutes and a slow stage with a separation speed of about  $1 \text{ km s}^{-1}$  lasting for 2 hr. We then estimate the rate of the magnetic reconnection in the corona, as represented by the electric fields  $E_c$  in the reconnecting current sheet, by measuring the ribbon motion speed and the magnetic fields obtained from MDI. We find that there were two stages as well in evolution of the electric fields:  $E_c = 1 \text{ V cm}^{-1}$  averaged over 20 minutes in the early stage, followed by  $E_c = 0.1 \text{ V cm}^{-1}$  in the subsequent 2 hr. The two stages of the ribbon motion and electric fields coincide with the impulsive and decaying phases of the flare, respectively, yielding clear evidence that the impulsive flare energy release is governed by the fast magnetic reconnection in the corona. We also measure the projected heights of the erupting filament from KSO  $H\alpha$  and *SOHO*/EIT images. The filament started to rise 20 minutes before the flare. After the flare onset, it was accelerated quickly at a rate of  $300 \text{ m s}^{-2}$ , and in 20 minutes, reached a speed of at least  $540 \text{ km s}^{-1}$ , when it disappeared beyond the limb in the EIT observations. The acceleration rate of the CME is estimated to be  $58 \text{ m s}^{-2}$  during the decay phase of the flare. The comparison of the height and velocity profiles between the filament and CME suggests that fast acceleration of mass ejections occurred during the impulsive phase of the flare, when the magnetic reconnection rate was also large, with  $E_c = 1 \text{ V cm}^{-1}$ .

*Subject heading:* Sun: activity — Sun: coronal mass ejections (CMEs) — Sun: filaments — Sun: flares — Sun: magnetic fields

### 1. INTRODUCTION

Eruptive two-ribbon flares provide a lot of information on the physical picture of the eruptive solar phenomena. Since the 1970s, some have suggested that two-ribbon flares are caused by magnetic reconnection between coronal field lines that are forced open by erupting filaments (see a review by Svestka & Cliver 1992). In the last two decades, the discovery and numerous studies of the coronal mass ejections (CMEs) and their relationship, specifically with long-duration two-ribbon flares and filament eruptions, has led to the idea that CMEs provide a powerful mechanism to stretch the coronal magnetic fields into an open configuration for magnetic reconnection to occur subsequently (Hundhausen 1988, 1999; Harrison et al. 1990; Low 1996 and references therein). Hundhausen and colleagues have proposed that the CME opens the field rather than the erupting filament: backward extrapolations of velocity diagrams indicate that the CME probably begins before the filament eruption and has stronger magnetic fields and more potential and kinetic energy than the erupting filament. Very recently, the simulation by Cheng et al. (2003) showed that flux rope's accelerated rising motion enhanced the magnetic reconnection rate.

The often-observed flare ribbon expansion is the chromospheric signature of the progressive magnetic reconnection

in the corona, in which new field lines reconnect at higher and higher altitudes. How quickly the ribbon expands in the chromosphere is then related to how fast the reconnection proceeds in the corona. Since the magnetic reconnection in the corona is hardly observable directly, many chromospheric observations have been conducted and analyzed in an effort to indirectly map the coronal magnetic reconnection (Schmieder et al. 1987; Svestka 1989; Falchi, Qiu, & Cauzzi 1997; Qiu et al. 2002).

Physically speaking, the velocity of the footpoint motion sweeping through the magnetic field lines corresponds to the rate of the magnetic flux convected into the diffusion region at the reconnection point in the corona, where the reconnecting current sheet (RCS) is generated. With some assumptions and approximations, Forbes and colleagues (Forbes & Priest 1984; Forbes & Lin 2000) derive a very simple relationship between the electric field strength ( $E_c$ ) along the current sheet and two observables,  $V_t$  and  $B_n$ , as  $E_c = V_t B_n$ , where  $B_n$  is the normal component of magnetic field strength of the ribbon and  $V_t$  represents the transverse velocity of the flare ribbon motion. In the past, very few attempts have been made to explore the electrical field in the RCS from the flare footpoint kernel motion. Using the above relation, Poletto & Kopp (1986) derived the maximum  $E_c$  of  $2 \text{ V cm}^{-1}$  in a large two-ribbon flare. Recently, Qiu et al. (2002) studied an impulsive flare with high cadence  $H\alpha$  observations at Big Bear Solar Observatory (BBSO). They estimated the maximum electric field at RCS to be  $90 \text{ V cm}^{-1}$ , which occurred around the peaking time of hard X-rays. The derived  $E_c$  is proportional to the magnetic reconnection rate, which is fundamentally controlled by the coronal magnetic fields and dynamics.

<sup>1</sup> National Astronomical Observatory of China, Beijing, China; haimin@flare.njit.edu.

<sup>2</sup> Big Bear Solar Observatory, New Jersey Institute of Technology, 40386 North Shore Lane, Big Bear City, CA 92314-9672.

<sup>3</sup> Center for Solar Research, New Jersey Institute of Technology, Newark, NJ 07102.

The association between eruptive two-ribbon flares and coronal mass ejections (CMEs) is frequently addressed, although so far, most observations failed to establish a systematic correlation among the onset of solar flares, filament eruptions, and CMEs (Verma 1990; Feynman & Hundhausen 1994; Harrison 1995; McAllister et al. 1996). Detecting the early manifestation of CMEs on the solar disk and their relationship with solar surface phenomena is essential to understanding the physical origin of CMEs. Theoretically, there are two kinds of CME models that also underline different flare-CME relationships. In the flux-rope model (Forbes & Priest 1995; Amari et al. 2000), mass ejections force open the magnetic field arcade, leaving behind large-scale magnetic reconnection between open-field lines. The subsequent feedback of the magnetic reconnection to the mass ejection is discussed by Lin & Forbes (2000). In the break-out model (Antiochos, DeVore, & Klimchuk 1999), magnetic reconnection occurs first to open the coronal magnetic structure for mass to escape. Therefore, in this model, the magnetic reconnection precedes the mass ejection, and how quickly the mass moves out of the surface system should be related to how rapidly the magnetic reconnection proceeds. These two models depict different magnetic configurations that also regulate the energy budget carried by mass ejections and released by dissipation via magnetic reconnection. Although demanding, the models need to be tested by observations that compare the dynamics of the mass ejection and the magnetic reconnection responsible for flare energy release (Zhang et al. 2001).

In this paper, we present the result on the analysis of a quiet-Sun flare associated with an erupting filament and a

fast CME. The flare exhibits a clear two-ribbon separation motion over several hours, which can be used to infer the evolution of the coronal magnetic reconnection. We select this clear case to avoid complex magnetic structures. The Kanzelhöhe Solar Observatory (KSO) and *Solar and Heliospheric Observatory (SOHO)* observations also provide continuous observations of the filament activation and eruption, which can be used to infer the dynamics of the CME at its takeoff. Combinations of ribbon separation and filament/CME height would give us a three-dimensional physical picture associated with the eruptive flare. It is also possible to investigate the physical connection between the flare dynamics, filament eruption, and CME quantitatively.

## 2. OBSERVATIONS AND DATA REDUCTION

In the past 2.5 yr, we have successfully installed and are continuously operating a high-resolution global  $H\alpha$  network. The stations are at BBSO, KSO in Austria, Catania Astrophysical Observatory (CAO) in Italy, Yunnan Observatory (YO), and Huairou Solar Observing Station (HSOS) in China. Nominally, each station obtains  $H\alpha$  image every minute with a  $1''$  pixel resolution. The data are calibrated using standard procedures at BBSO.

The primary data source used in the current study are from full-disk  $H\alpha$  data obtained from KSO station on 2000 September 12. KSO had complete coverage of the M1 flare and the associated filament eruption at about 12 UT. Figure 1 is the time sequence of KSO  $H\alpha$  images showing the evolution of the event. It is a classical two-ribbon flare accompanied by the filament eruption.

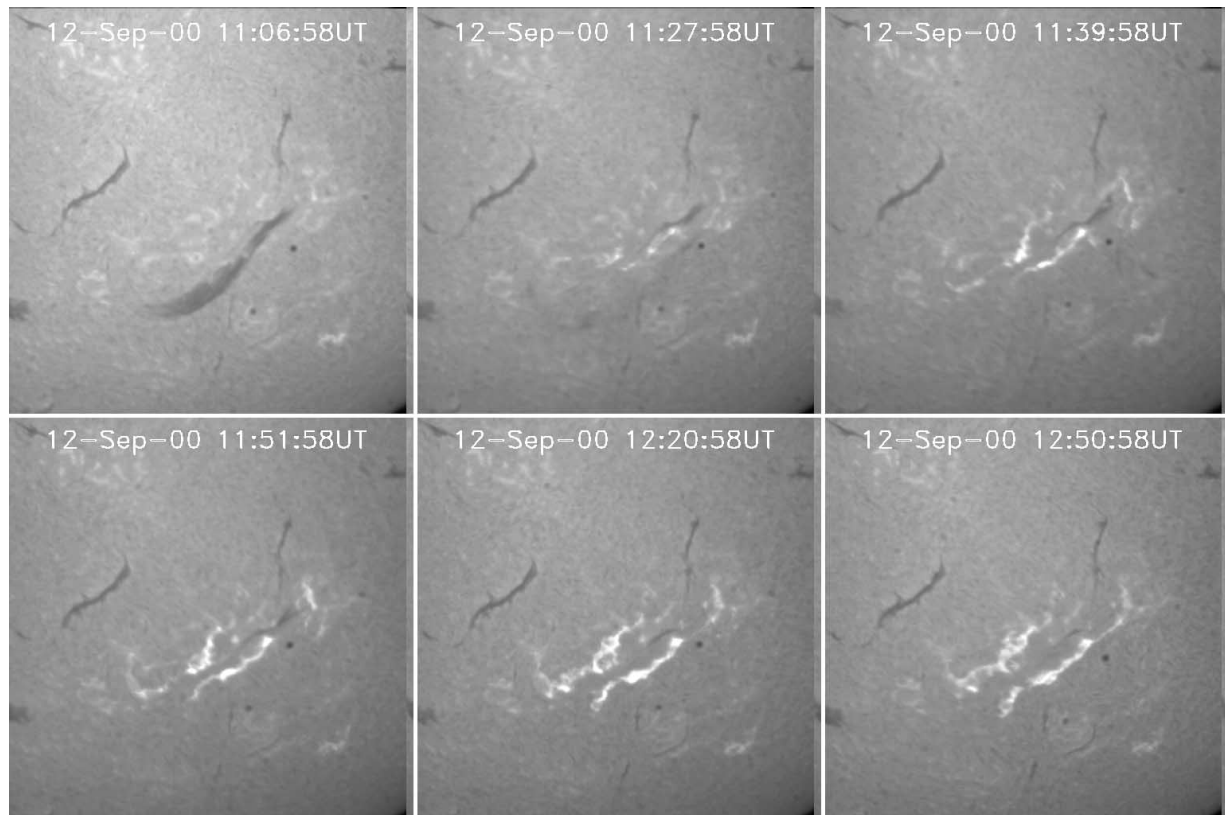


FIG. 1.—Sequence of  $H\alpha$  images showing the evolution of the flare and the disappearance of filament. Field of view is  $512'' \times 512''$ .

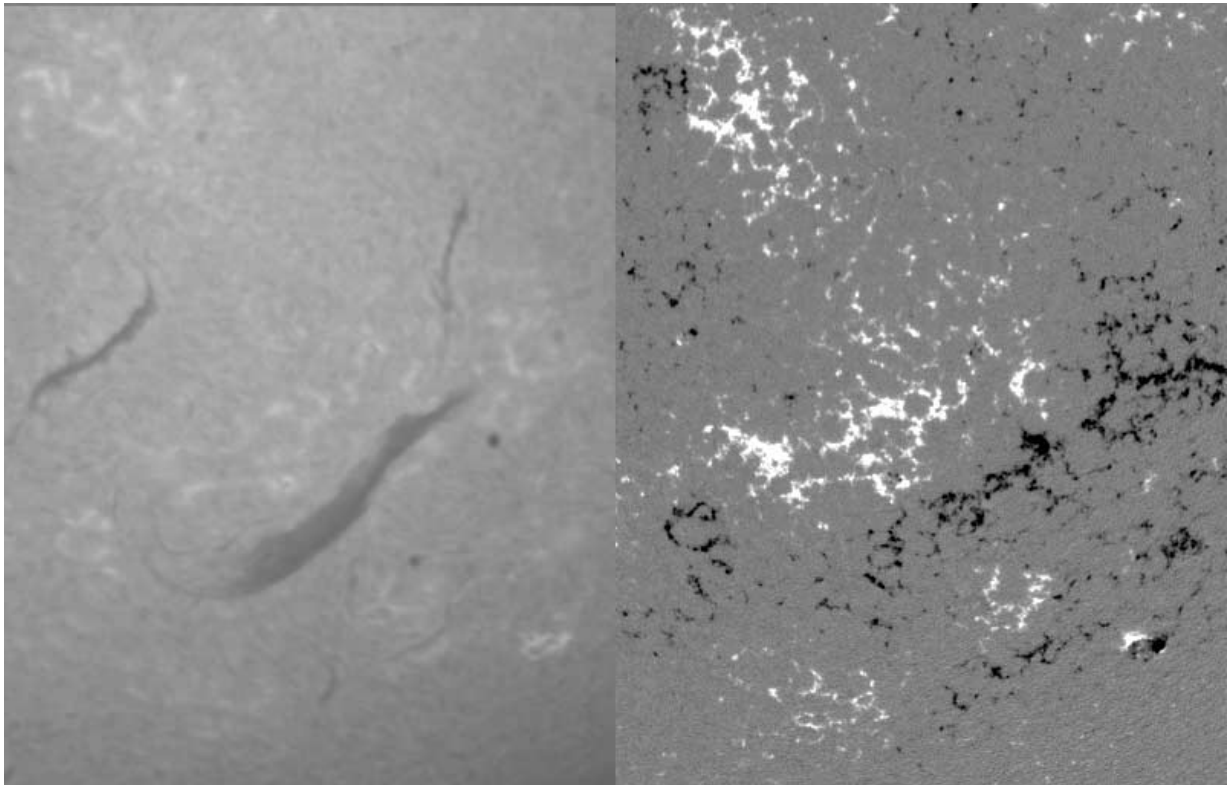


FIG. 2.—Comparison of a  $H\alpha$  image with corresponding magnetogram at 1000 UT

The same event was covered by *SOHO* EIT, MDI, and LASCO observations. It is clearly associated with a fast halo CME. MDI data provides full-disk magnetograms, which are aligned with  $H\alpha$  data for the study of magnetic properties of moving ribbons. Figure 2 compares the  $H\alpha$  image during the flare and the corresponding MDI magnetogram.

### 3. RESULTS

#### 3.1. Dynamical Evolution

We first study the temporal evolution of the flare ribbon separation, filament eruption, and CME height with respect to flare energy release. In Figure 3, we plot the time profiles of the flare emission, ribbon separation distance, and heights of the filament and CME. We fit these distance/height profiles to hyperbolic functions of time and derive and compare their velocity profiles in Figure 4. The *GOES* soft X-ray light curve is used to represent the time profile of the flare energy release. To investigate the electron acceleration in the impulsive phase of the flare, the hard X-ray and microwave observations are essential. Unfortunately, we did not have such data. We therefore use the time derivative of the *GOES* soft X-ray light curve to represent the hard X-ray time profile, assuming that the so-called Neupert effect is valid in this event.

In the top panel of Figure 3, we plot the *GOES* soft X-ray light curve of 1–8 Å and its derivative. The middle panel shows the average ribbon separation distance as a function of time. The position of the ribbon was defined by the location of the moving front. This flare exhibits a rather regular pattern of ribbon-separation motion, with both ribbons

moving away from and nearly perpendicular to the magnetic neutral line. Therefore, there is only a small ambiguity in the measurement of the separation motion. As we can see from Figures 3 and 4, there are two stages in the ribbon-separation motion: a fast separation stage in the first 20 minutes of the event and a substantially slower stage afterward. The fast stage coincides with the rising phase of the derivative of the soft X-ray light curve, i.e., the impulsive phase of the flare energy release when most of the flare non-thermal electrons are accelerated. On average, the speed of the ribbon separation during the impulsive phase of the flare is over  $10 \text{ km s}^{-1}$ , and the average speed in the later stage is about  $1 \text{ km s}^{-1}$ . Our observations therefore indicate that the fast ribbon motion corresponds to a greater energy-release rate.

Then let us take a look at the erupting filament and halo CME. In the lower two panels of Figure 3, we plot the heights of the filament and CME front. The solid line denotes the measurements of the filament height in  $H\alpha$  images with 1 minute cadence, and the plus symbols represent measurements from EIT 195 Å images with a 12 minute cadence. The measurement was not easy because the contrast of the filament decreased rapidly as it moved up. We measured the lateral displacement and project it to the vertical direction on the basis of the disk position of the filament. Of course, we had to assume that the filament moved up exactly vertically in the local solar coordinate system. Given the uncertainties in the measurements, the figure shows that the filament height profiles measured from the two kinds of images are consistent. The fits to the filament heights and the velocity profiles are shown in Figure 4. The filament started to rise about 30 minutes before the appearance of

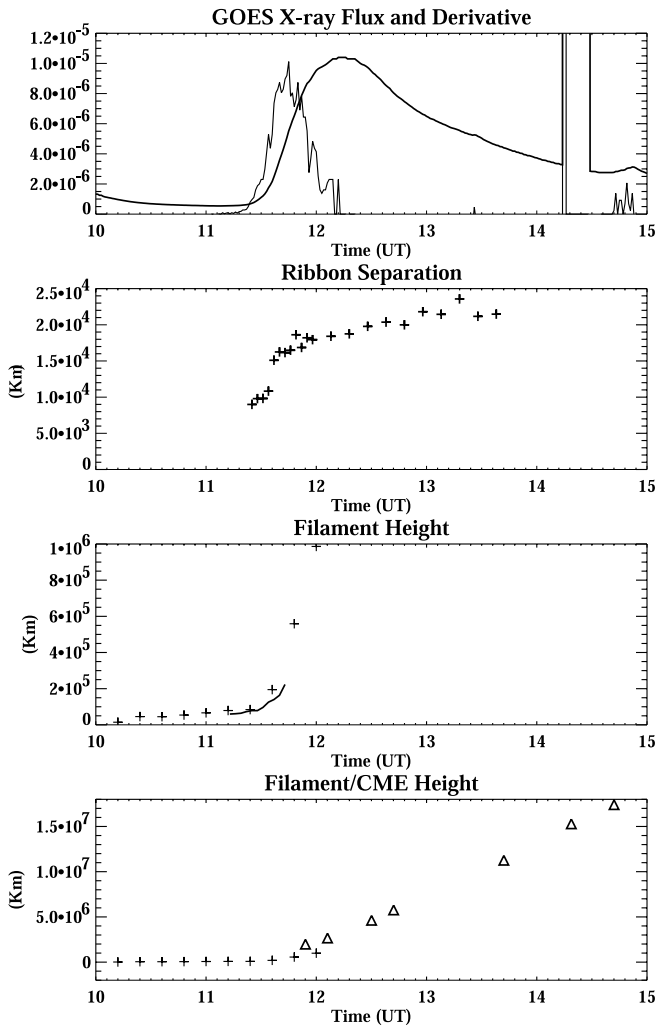


FIG. 3.—*Top panel:* GOES X-ray flux and its derivative (thinner line) as a function of time in the energy channel of 1–8. *Upper middle panel:* Mean flare ribbon separation as a function of time. *Lower middle panel:* Filament height as a function of time. *Solid lines:* KSO  $H\alpha$  measurements and the pluses are from SOHO EIT measurements. *Bottom panel:* EIT filament height and LASCO CME height.

the flare ribbons, reaching a velocity of several tens of  $\text{km s}^{-1}$ . However, after the flare onset ( $\sim 1120$  UT), it was rapidly accelerated to over  $200 \text{ km s}^{-1}$  before becoming invisible in  $H\alpha$  ( $\sim 1140$  UT) and to at least  $540 \text{ km s}^{-1}$ , when it moved beyond the limb in the EIT field of view around 12 UT.

The triangle symbols in the bottom panel of Figure 3 indicate the heights of the associated halo CME front measured by Seiji Yashiro.<sup>4</sup> According to his measurements, the CME was first seen in LASCO C2 field at 1154 UT, and the front speed measured from a linear fit is  $1500 \text{ km s}^{-1}$ . Because of the limited fields of view of EIT and LASCO, one cannot identify the filament and CME in the same image. However, EIT and LASCO observations overlapped at around 12 UT, when the filament and CME were observed by the two instruments separately. Seen in Figure 4a, at this time, the displacement between the filament and CME is about

1.4–2 solar radii, taking into account the projection effects. This gives roughly the scale of the expanding system at that time.

With certain assumptions, the above observations also allow us to reasonably estimate the acceleration rate of the CME at its takeoff in several ways. In the first way, we may treat the filament eruption and CME as mass ejections driven by the same mechanism in the same system at the early stage of the mass ejections. Estimated from the velocity profiles in Figure 4b, from 1100 to 1200 UT, the average acceleration rate was  $260 \text{ m s}^{-2}$ . The filament was not accelerated at a constant rate. From 1140 to 1200 UT, the average acceleration rate reached  $380 \text{ m s}^{-2}$ . In the second way, we may note that the CME took off at 11 UT, when the filament was observed rising in the EIT field of view. Accordingly, to accelerate the CME to  $1270 \text{ km s}^{-1}$  at around 12 UT requires an average acceleration rate of  $350 \text{ m s}^{-2}$ . The acceleration rates estimated from these two methods are basically consistent, with the CME acceleration rate possibly a little higher than the filament due to the rapid expansion of the system. After 12 UT, the acceleration rate of the CME was estimated to be  $58 \text{ m s}^{-2}$  using the hyperbolic fit of the CME velocity profile in Figure 4b. S. Yashiro also estimated the CME acceleration rate to be  $58 \text{ m s}^{-2}$  from a second-order fit of the height-time profiles. These estimates suggest that fast acceleration of the mass ejections occurred before 12 UT, most likely during the impulsive phase of the flare. The rate of the fast acceleration is about 5 times that of the slow acceleration. This result is consistent with Zhang et al. (2001), yet our measurements are made with a better data coverage, under the assumption that the erupting filament and CME can be regarded as being accelerated in the same framework.

### 3.2. Electric Field along the Current Sheet

Our results in the last section show that the speed of the ribbon separation resembles the rate of the flare energy release through magnetic reconnection. It is also of our interest to explore the spatiality of the ribbon motion representative of the energy release rate from the observational point of view. For this purpose, we track the separation speed at all locations along the ribbon as a function of time. We find that the speed of the separation was not uniform along the flare ribbon, but at every point, the motion exhibits the same evolution pattern as the averaged separation mode shown in Figures 3 and 4. Therefore, we divide the data into two time bins: fast and slow separation stages. In Figure 5, we plot the speeds of the ribbon motion (away from the magnetic neutral lines) as a function of position along the ribbon. The positive and negative numbers represent the upper (north) and lower (south) ribbons, respectively. The thick lines represent the fast-moving stage corresponding to the impulsive phase of the flare, and thin lines, the slow-moving stage during the decay phase of the flare. In the first stage, the maximum speed  $V_i$  along the ribbon was over  $10 \text{ km s}^{-1}$ , while in the following stage, the maximum  $V_i$  was about  $1 \text{ km s}^{-1}$ .

Forbes & Priest (1984) and Forbes & Lin (2000) suggested that the ribbon motion can be used to infer the electric field  $E_c$  of the coronal current sheet in a two-dimensional assumption. In the middle and bottom panels of Figure 5, we plot the derived electric field  $E_c = V_i B_n$  as a function of ribbon position by assuming that, at each point along the

<sup>4</sup> For more information about this work, go to [http://cdaw.gsfc.nasa.gov/CME\\_list/](http://cdaw.gsfc.nasa.gov/CME_list/).

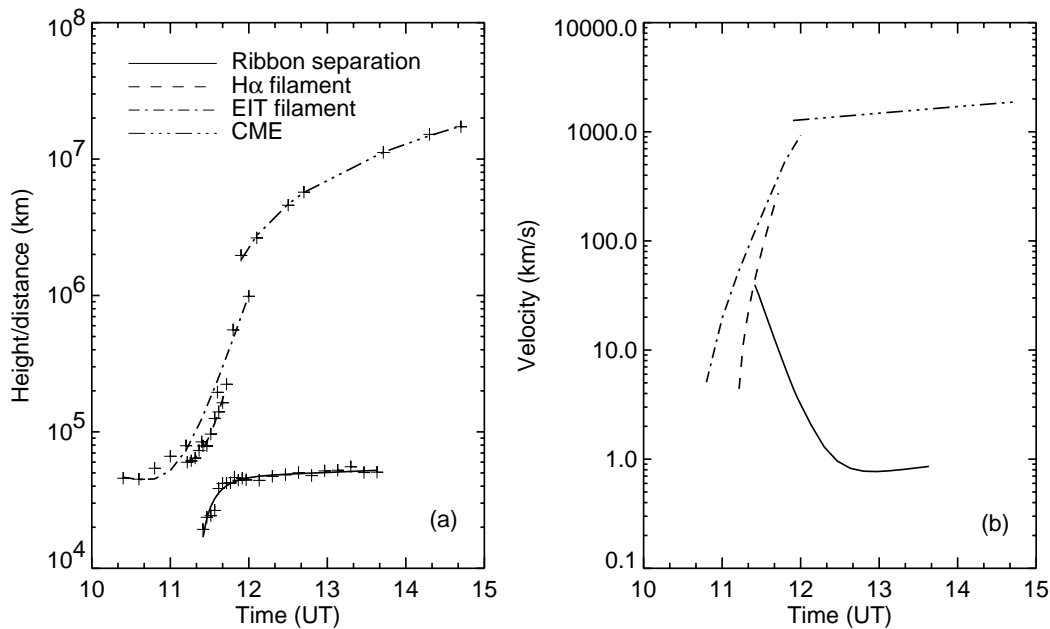


FIG. 4.—*Left*: Time profiles of the flare ribbon separation, filament heights measured from KSO and EIT images, and CME heights measured by S. Yashiro. *Lines*: Least-squares fits to hyperbolic functions. *Right*: Velocity profiles of the ribbon separation, filament, and CME derived from the fits of the height profiles.

ribbon (or along the arcade axis), the two-dimensional approximation is still valid. The line-of-sight magnetic field  $B_n$  was measured from MDI observations. First, we find that the evolution of  $E_c$  exhibits the same pattern as the speed. During the early time bin, the flare has a much stronger electric field of the order of  $1 \text{ V cm}^{-1}$  on average, while in the later time bin,  $E_c$  is around  $0.1 \text{ V cm}^{-1}$ . Since  $E_c$  is proportional to the magnetic reconnection rate at the reconnecting point, our results confirm that the flare energy release is most efficient when the magnetic reconnection rate is also big. During the decay phase lasting for about 2 hr, the magnetic reconnection still continues at a slow rate. Second, Figure 5 shows that  $E_c$  is inhomogeneous along the ribbon, most likely indicating the inhomogeneity in the magnetic reconnection rate along the ribbon. Such inhomogeneity should be determined by the magnetic configuration in the corona.

The values of the electric field derived for this event are much smaller than  $90 \text{ V cm}^{-1}$  as derived by Qiu et al. (2002) but are comparable to the value by Polletto & Kopp (1986). According to these values, the electric fields in the current sheet in these events are super-Dreicer fields in which electrons can be efficiently accelerated. Unfortunately, there were no hard X-ray observations to allow further studies on the thermal/nonthermal properties of accelerated electrons. Concerning the large difference between the results for this event and the values by Qiu et al. (2002), we recognize a few points in deriving  $E_c$ . First, Qiu et al. used data with much higher cadence, and the ribbon separation motion in their study is much faster. Second, in Qiu et al. (2002), the flare occurred in strong magnetic fields. Whereas  $V_r$  is measured in the chromosphere,  $B_n$  is measured in the photosphere. In strong field regions, the magnetic fields may vary more drastically from the photosphere to the chromosphere, leading to an overestimate of the electric fields in Qiu et al. (2002). The event studied in this paper occurred in the decayed

region, where the magnetic fields are rather diffuse, yielding a relatively smaller error than the estimates by Qiu et al. (2002).

#### 4. CONCLUSIONS AND DISCUSSIONS

In this paper, we present the detailed study on the temporal and spatial properties of a quiet-Sun two-ribbon flare. This event exhibits a good example of a standard solar flare characterized by the long duration, filament eruption, two-ribbon separation, and its association with a fast CME. Observations from various instruments provide an almost complete coverage of the dynamic evolution of this event. The most important result is the difference between the two evolution stages of the event, which is evident in several aspects.

We studied the separation of flare ribbons observed at the chromosphere as a function of time and found that there were two stages of separation: a rapid stage at a speed of about  $10 \text{ km s}^{-1}$  in the first 20 minutes, corresponding to the impulsive phase of the flare energy release, and a much slower speed of about  $1 \text{ km s}^{-1}$  at the later stage, lasting for more than 1.5 hr when flare emission decayed. These numbers are similar to the values derived for the 1973 July 29 two-ribbon flare (Moore et al. 1980; Svestka et al. 1982).

We derived the electric fields by measuring the ribbon motion and the magnetic fields along the ribbon. We found the average electric fields at the two evolution stages to be  $1$  and  $0.1 \text{ V cm}^{-1}$ , respectively. As the rise of the flare emission coincides with the duration of the strong electric field, we therefore conclude that the impulsive flare energy release occurred when the electric field was in the order of  $1 \text{ V cm}^{-1}$ . The sudden drop in the electric field is not due to the fact that flare ribbons hit a strong magnetic field region and stopped the motion. Instead, the ribbon motion in the chromosphere was a consequence of the evolution of the

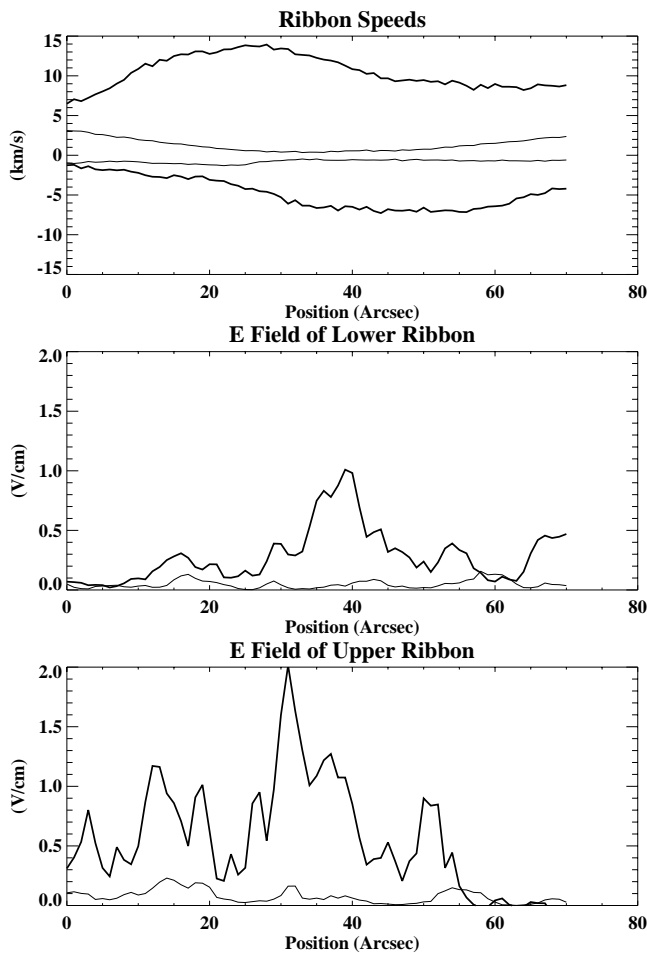


FIG. 5.—*Top panel:* Mean ribbon moving speeds along ribbons. *Thick lines:* Time period of 1125–1200 UT (time bin 1). *Thin lines:* Time period of 1200–1350 UT (time bin 2). *Middle and bottom panels:* Derived electric fields for the lower and upper panels, respectively. The electric fields are derived from the ribbon moving speed and line-of-sight magnetic fields measured at the location of ribbons.

magnetic reconnection in the corona, which consisted of a fast stage and a slow stage in this event. In general, the result of the two-stage electric current agrees with the modeling of Lin et al. (1995). However, the details need to be mapped out by case-specific models.

We also studied the projected heights of the erupting filament, finding that with available observations, the erupting filament was rapidly accelerated to over  $540 \text{ km s}^{-1}$  during the impulsive phase of the flare, which is very close to the escape velocity. Comparing the time profiles of the flare emission, ribbon motion, and the height of the top of filament, we believe that magnetic reconnection was switched on when the filament was in the height range of  $1.5 \times 10^5$  to  $2.5 \times 10^5 \text{ km}$ . Around this time, we also observed the onset of fast acceleration of the filament mass.

Comparing the velocity profiles of the filament and CME, it is also likely that fast acceleration of the mass ejections, with an acceleration rate of over  $300 \text{ m s}^{-2}$ , coincided with the flare impulsive phase with a large magnetic reconnection rate, as represented by the strong electric field. During the long decay of the flare, when the magnetic reconnection rate reduced by an order of magnitude, the acceleration rate of the mass ejections dropped to  $58 \text{ m s}^{-2}$ .

The parameters derived in this study for the two-stage evolution of the dynamics and magnetic reconnection should provide information for theoretic modeling. A few questions are raised from this study, and seeking their answers may help reveal the underlying physics. First, the two evolution stages are distinguished by the sudden switch of the electric field amplitude and mass acceleration rate. What is the mechanism of such switch? Is it due to a sudden change in the magnetic configuration, such as opening of the magnetic field lines, at that particular time? What is the physics behind the apparent coincidence between the magnetic reconnection rate and the dynamical evolution of the mass ejections? Second, apart from the two-stage evolution, Figure 4b also shows that during the first stage, while the velocity profile of the filament shows the filament being accelerated, the velocity profile of the ribbon motion suggests a deceleration. From an observational point of view, we should enlarge the sample of such studies to understand whether such anticorrelation can be established or if it is purely an accident due to uncertainties in data analysis. Theoretically, shall we or shall we not expect such results?

Answers to these questions are important for understanding the physical mechanisms governing the dynamical evolution and magnetic reconnection in eruptive solar events. Some CME models have been presented that do not involve magnetic reconnection (e.g., Low 1994), but in many other cases, CMEs and flares are associated in a way yet unclear to us. In the first place, even given the sharp contrast between the spatial scales of CMEs and flares, the radiative energy in a typical eruptive flare, which is released mainly through magnetic reconnection, is comparable to the kinetic energy carried by ejected masses. More importantly, even though past studies have found it hard to conceive a causal relationship between flares and CMEs, the intriguing question remains of what role the magnetic reconnection plays in the framework of the large-scale eruption. The configurations invoked by both the flux rope and break-out models, if correctly depicting the real situation, would naturally address the link between the rate of the magnetic reconnection and the rate of mass acceleration, at least during the early stage of the event, because the laws of magnetic flux and mass conservation are to be observed. The direct relationship between the two, such as the time profiles of magnetic reconnection and CME acceleration, may be calculated given a specific magnetic configuration.

A somewhat different but not unrelated issue raised in this study also deserves further investigation in the future. In Figure 5, one can see that the amplitude of the electric field, nominally representative of the magnetic reconnection rate, is not uniform along flare ribbons, indicating a large inhomogeneity in the coronal magnetic reconnection. So far, theoretical models mentioned above only deal with two and a half-dimensional configurations with a translational symmetry along the axis of the arcade. Our observations show that, at least in the case of the magnetic reconnection, such a translational symmetry may not exist. Taking into consideration the real three-dimensional configuration may result in some different theoretical arguments. Furthermore, very recently, Asai et al. (2002) found that hard X-ray sources only concentrate in some parts of an  $H\alpha$  radiation source, where the magnetic fields, and consequently, the magnetic reconnection rates, are strong. It is interesting to derive the electric fields at these locations to compare with other locations along the ribbon. It is also worth comparing with

other events for which the photospheric magnetic fields are more homogeneous, in order to understand what agent controls the magnetic reconnection rate.

We are grateful to the KSO observing staff for their support in obtaining the data. We thank J. Lin for helpful discussion and the referee for valuable comments. The work is

supported by NSF under grants ATM-0076602, ATM-0233931, and AST 99-87366, NASA grants NAG5-10910 and NAG5-12733, ONR grant N00014-03-1-0093, and the Chinese NSF. The first draft of the paper was finished while H. W. was visiting the National Astronomical Observatory of China. He wishes to thank the staff of the observatory for their support.

## REFERENCES

- Amari, T., Luciani, J. F., Mikic, Z., & Linker, J. 2000, *ApJ*, 529, L49  
 Antiochos, S. K., DeVore, C. R., & Klimchuk, J. A. 1999, *ApJ*, 510, 485  
 Asai, A., Masuda, S., Yokoyama, T., Shimojo, M., Isobe, H., Kurokawa, H., & Shibata, K. 2002, *ApJ*, 578, L91  
 Cheng, C. Z., Ren, Y., Choe, G. S., & Moon, Y. J. 2003, *ApJ*, submitted  
 Falchi, A., Qiu, J., & Cauzzi, G. 1997, *A&A*, 328, 371  
 Feynman, J., & Hundhausen, A. J. 1994, *J. Geophys. Res.*, 99, 8451  
 Forbes, T. G., & Lin, J. 2000, *J. Atmos. Sol.-Terr. Phys.*, 62, 1499  
 Forbes, T. G., & Priest, E. R. 1984, in *Solar Terrestrial Physics: Present and Future*, ed. D. M. Butler & K. Paradopoulos (Greenbelt: NASA), 1  
 ———. 1995, *ApJ*, 446, 377  
 Harrison, R. A. 1995, *A&A*, 304, 585  
 Harrison, R. A., Hildner, E., Hundhausen, A. J., Sime, D. G., & Simnett, G. M. 1990, *J. Geophys. Res.*, 95, 917  
 Hundhausen, A. J. 1988, in *Proc. 6 International Solar Wind Conf.*, ed. V. Pizzo, D. G. Sime, & T. E. Holzer (Boulder: NCAR), 181  
 ———. 1999, in *The Many Faces of the Sun: A Summary of the Results from NASA's Solar Maximum Mission*, ed. K. T. Strong, et al. (New York: Springer), 143  
 Lin, J., & Forbes, T. G. 2000, *J. Geophys. Res.*, 105, 2375  
 Lin, J., Forbes, T. G., Priest, E. R., & Bungey, T. N. 1995, *Sol. Phys.*, 159, 275  
 Low, B. C. 1994, *Plasma Phys.*, 1, 1684  
 ———. 1996, *Sol. Phys.*, 167, 217  
 McAllister, A. H., Dryer, M., McIntosh, P., Singer, H., & Weiss, L. 1996, *J. Geophys. Res.*, 101, 13  
 Moore, R. L., et al. 1980, in *Solar Flares*, ed. P. Sturrock (Boulder: Univ. Colorado Press), 341  
 Polletto, G., & Kopp, R. A. 1986, in *The Lower Atmosphere of Solar Flares*, ed. D. F. Neidig (Sunspot: NSO), 453  
 Qiu, J., Lee, J., Gary, D. E., & Wang, H. 2002, *ApJ*, 565, 1335  
 Schmieder, B., Forbes, T. G., Malherbe, J. M., & Machado, M. E. 1987, *ApJ*, 317, 956  
 Svestka, Z. 1989, *Sol. Phys.*, 121, 399  
 Svestka, Z., & Cliver, E. W. 1992, in *Eruptive Solar Flares*, ed. Z. Svestka et al. (Berlin: Springer), 1  
 Svestka, Z., Dodson-Prince, H. W., Martin, S. F., Mohler, O. C., Nolte, L. T., & Petraso, R. D. 1982, *Sol. Phys.*, 78, 271  
 Verma, V. K. 1990, in *IAU Symp. 142, Basic Plasma Processes on the Sun*, ed. E. R. Priest & V. Krishan (San Francisco: ASP), 450  
 Zhang, J., Dere, K. P., Howard, R. A., Kundu, M. R., & White, S. M. 2001, *ApJ*, 559, 452